

Computing the ground state solution of Bose-Einstein condensates by an energy-minimizing normalized residual network

Ren-Tao Wu(吴任涛), Ji-Dong Gao(高济东), Yu-Han Wang(王宇晗), Zhen-Wei Deng(邓振威), Ming-Jun Li(李明军), and Rong-Pei Zhang(张荣培)

Citation: Chin. Phys. B, 2025, 34 (**10**): 100305. DOI: 10.1088/1674-1056/ade062
http://cpb.iphy.ac.cn; http://iopscience.iop.org/cpb

What follows is a list of articles you may be interested in

Ground state of SU(3) spin-orbit coupled soft-core Bose gas

Jia Liu(刘佳), Jing Feng(冯婧), Ya-Jun Wang(王雅君), Xiao-Fei Zhang(张晓斐), and Xue-Ying Yang(杨雪滢)
Chin. Phys. B, 2025, 34 (**6**): 060301. DOI: 10.1088/1674-1056/adc36b

Bessel vortices in spin-1 Bose-Einstein condensates with Zeeman splitting and spin-orbit coupling

Huan-Bo Luo(罗焕波), Xin-Feng Zhang(张鑫锋), Runhua Li(李润华), Yongyao Li(黎永耀), and Bin Liu(刘彬)
Chin. Phys. B, 2024, 33 (**10**): 100304. DOI: 10.1088/1674-1056/ad6424

Effects of drive imbalance on the particle emission from a Bose-Einstein condensate in a one-dimensional lattice

Long-Quan Lai(赖龙泉) and Zhao Li(李照)
Chin. Phys. B, 2024, 33 (**3**): 030308. DOI: 10.1088/1674-1056/ad1172

Enhanced measurement precision with continuous interrogation during dynamical decoupling

Jun Zhang(张军), Peng Du(杜鹏), Lei Jing(敬雷), Peng Xu(徐鹏), Li You(尤力), and Wenxian Zhang(张文献)
Chin. Phys. B, 2024, 33 (**3**): 030301. DOI: 10.1088/1674-1056/ad1985

Dynamical nonlinear excitations induced by interaction quench in a two-dimensional box-trapped Bose-Einstein condensate

Zhen-Xia Niu(牛真霞) and Chao Gao(高超)
Chin. Phys. B, 2024, 33 (**2**): 020314. DOI: 10.1088/1674-1056/ad1179

Computing the ground state solution of Bose–Einstein condensates by an energy-minimizing normalized residual network

Ren-Tao Wu(吴任涛)[1], Ji-Dong Gao(高济东)[1], Yu-Han Wang(王宇晗)[1], Zhen-Wei Deng(邓振威)[1], Ming-Jun Li(李明军)[2], and Rong-Pei Zhang(张荣培)[1,†]

[1] *School of Advanced Manufacturing, Guangdong University of Technology, Jieyang* 522000, *China*
[2] *School of Mathematics and Computational Science, Xiangtan University, Xiangtang* 411105, *China*

(Received 19 February 2025; revised manuscript received 17 May 2025; accepted manuscript online 4 June 2025)

This paper introduces a novel numerical method based on an energy-minimizing normalized residual network (EM-NormResNet) to compute the ground-state solution of Bose–Einstein condensates at zero or low temperatures. Starting from the three-dimensional Gross–Pitaevskii equation (GPE), we reduce it to the 1D and 2D GPEs because of the radial symmetry and cylindrical symmetry. The ground-state solution is formulated by minimizing the energy functional under constraints, which is directly solved using the EM-NormResNet approach. The paper provides detailed solutions for the ground states in 1D, 2D (with radial symmetry), and 3D (with cylindrical symmetry). We use the Thomas–Fermi approximation as the target function to pre-train the neural network. Then, the formal network is trained using the energy minimization method. In contrast to traditional numerical methods, our neural network approach introduces two key innovations: (i) a novel normalization technique designed for high-dimensional systems within an energy-based loss function; (ii) improved training efficiency and model robustness by incorporating gradient stabilization techniques into residual networks. Extensive numerical experiments validate the method's accuracy across different spatial dimensions.

Keywords: Bose–Einstein condensate, Gross–Pitaevskii equation, energy minimization, normalized residual network

PACS: 03.75.Hh, 07.05.Mh, 02.60.Lj

DOI: 10.1088/1674-1056/ade062 **CSTR:** 32038.14.CPB.ade062

1. Introduction

Bose–Einstein condensates (BECs) represent a quantum phase transition that occurs at ultralow temperatures, where a macroscopic number of bosons occupy the same quantum ground state. This collective behavior gives rise to remarkable macroscopic quantum phenomena, including superfluidity and quantum entanglement.[1] The theoretical foundation of BECs was established by Albert Einstein in 1924, building upon Satyendra Nath Bose's statistical formulation for photons. This prediction was experimentally verified in 1995 with the realization of BECs in single-component atomic gases.[2]

At zero-temperature, a dilute BEC is described by a macroscopic complex wave function that defines the condensate's order parameter. Its spatiotemporal evolution is governed by the Gross–Pitaevskii equation (GPE).[3] The GPE accurately models BEC dynamics and is widely applied in nonlinear optics, cold atom physics, and plasma physics.[4–7]

The ground state of the GPE constitutes the lowest-energy solution to this nonlinear Schrödinger equation, characterizing the equilibrium state of a BEC at absolute zero temperature. This ground state is essential for both theoretical and experimental investigations of BECs, offering significant insights into their static and dynamic characteristics. Furthermore, it serves as a fundamental basis for advancing research in quantum physics, nonlinear dynamics, and applied quantum technologies.

Over the years, several numerical methods have been developed to address the ground-state problem of BECs. The most traditional approach is the imaginary-time evolution method,[8,9] iteratively optimizing the wave function through energy gradients flow. Other prevalent methods include constrained optimization techniques,[10] the time-splitting spectral method by Bao *et al.*,[4,12] and the Crank–Nicolson finite difference method utilized by Adhikari *et al.* and Caliari *et al.*[13,14]

Existing methods struggle to handle multi-dimensional systems with complex symmetries. The imaginary-time evolution method[9] performs well in one-dimensional or simple geometries but relies heavily on initial conditions and fails to converge globally in complex cases. The direct energy minimization method,[15] though effective for low-dimensional systems, requires extra for complex symmetry conditions.[16] Efficient numerical methods addressing these limitations remain crucial for GPE research.

Recent advances in machine learning enable efficient solutions for solving high-dimensional partial differential equations (PDEs). Physics-informed neural networks (PINNs)[17] integrate governing equations and boundary/initial conditions

†Corresponding author. E-mail: rongpei_zhang@gdut.edu.cn

© 2025 Chinese Physical Society and IOP Publishing Ltd. All rights, including for text and data mining, AI training, and similar technologies, are reserved.

into loss functions, eliminating mesh generation. Unlike traditional mesh-based methods, PINNs directly approximate solutions through parameter optimization, achieving computational efficiency in high-dimensional systems.[18–20] However, PINNs face two limitations: suboptimal accuracy due to the L_2 norm least-squares framework, and sensitivity to time sampling. Insufficient temporal resolution increases prediction errors and computational costs.

Inspired by the Deep Ritz method,[21] we develop a residual neural network-based framework[22] for the ground state solution. Residual blocks enhance the network's approximation capability. This paper presents two primary contributions. First, we design the loss function based on the energy functional, enabling the network to directly approximate the ground state during training. A novel normalization technique is introduced for high-dimensional systems with spherical symmetry. Second, we propose a stabilization factor in neural networks. Specifically, gradient clipping and scaling factors are applied to stabilize the training process, mitigate gradient-related issues, and improve the model's robustness and performance.

The remainder of this paper is organized as follows. Section 2 presents the introduction of the ground state and GPE. Section 3 offers a detailed description of the network method. Section 4 presents comprehensive numerical experiments that validate the accuracy of the proposed method. Finally, Section 5 concludes the paper with a summary of the findings.

2. Gross–Pitaevskii equation

The Gross–Pitaevskii equation (GPE) is a nonlinear Schrödinger equation that describes the macroscopic wavefunction $\psi(r,t)$ of a BEC at zero temperature:

$$\mathrm{i}\hbar\frac{\partial\psi}{\partial t}=\left(-\frac{\hbar^2}{2m}\nabla^2+V(\boldsymbol{x})+g|\psi|^2\right)\psi, \tag{1}$$

where $V(\boldsymbol{x})$ is the external potential energy, $\boldsymbol{x}=(x,y,z)$ is the spatial coordinate vector and g quantifies the interaction strength between atoms. The constant g is determined by the atomic mass (m), the s-wave scattering length a_{s} and Planck constant $(\hbar)$, as $g=4\pi\hbar a_{\mathrm{s}}/m$.

The wave function must be properly normalized to ensure that the total probability of finding the particle over all space is 1. The fundamental requirement of quantum mechanics is presented by the following equation:

$$\int_{\mathbb{R}^3}|\psi(\boldsymbol{x},t)|^2\,\mathrm{d}\boldsymbol{x}=1. \tag{2}$$

According to Bao and Tang,[15] the GPE (1) can be scaled under the normalization (2) into the following dimensionless form:

$$\mathrm{i}\frac{\partial\psi}{\partial t}=\left(-\frac{1}{2}\nabla^2+V(\boldsymbol{x})+\beta|\psi|^2\right)\psi. \tag{3}$$

This paper focuses on systems with radial or cylindrical symmetry, where the high-dimensional GPE can be simplified to the low-dimensional form, which simplifies the calculation while maintaining the physical fidelity.

2.1. The radially symmetric ground state

The GPE (3) reduces to the following 1D equation for the radial symmetry 2D problem and the spherical symmetry 3D problem:

$$\begin{aligned}\mathrm{i}\frac{\partial\psi(r,t)}{\partial t}&=-\frac{1}{2}\frac{1}{r^{d-1}}\frac{\partial}{\partial r}\left(r^{d-1}\frac{\partial}{\partial r}\psi(r,t)\right)\\&\quad+V(r)\psi(r,t)+\beta|\psi(r,t)|^2\psi(r,t),\end{aligned} \tag{4}$$

where $d=1,2,3$ and $V(r)$ is independent of angular coordinates.

Substituting $\psi(x,t)=\mathrm{e}^{-\mathrm{i}\mu t}\phi(x)$, we get the time-independent equation

$$-\frac{1}{2}\frac{1}{r^{d-1}}\frac{\mathrm{d}}{\mathrm{d}r}\left(r^{d-1}\frac{\mathrm{d}\phi}{\mathrm{d}r}\right)+V(r)\phi+\beta|\phi|^2\phi=\mu\phi. \tag{5}$$

It is required that $\phi(r,t)$ fulfills the normalization conditions

$$C_d\int_0^\infty|\phi(r)|^2r^{d-1}\,\mathrm{d}r=1. \tag{6}$$

The ground-state wave function is determined by solving the minimal eigenvalue problem (5), subject to a normalization condition (6) that ensures physical consistency. The energy functional $E(\phi)$ with radially symmetry is defined as

$$\begin{aligned}E(\phi)&=C_d\int_0^\infty r^{d-1}\left(\frac{1}{2}\left[\phi'(r)\right]^2\right.\\&\quad\left.+\frac{1}{2}r^2\phi^2(r)+\frac{\beta}{2}\phi^4(r)\right)\mathrm{d}r,\end{aligned} \tag{7}$$

where C_d is a normalization constant associated with dimension d, and its value depends on dimension d:

$$C_d=\begin{cases}2, & d=1,\\ 2\pi, & d=2,\\ 4\pi, & d=3.\end{cases} \tag{8}$$

The boundary conditions are set as $\partial\phi(0,t)/\partial r=0$ at the origin $r=0$, and $\phi(r,t)\to0$ for $r\to+\infty$.

Now we will prove that the ground state of the GPE (9) can be obtained by minimizing energy functional (7) under the normalization constraint (6), i.e.,

$$\phi_{\mathrm{g}}=\underset{\phi\in V}{\operatorname{argmin}}E(\phi). \tag{9}$$

First, we define the Lagrangian functional by introducing the chemical potential μ as a Lagrange multiplier,

$$\mathcal{L}[\phi]=E[\phi]-\mu\left(C_d\int_0^\infty|\phi(r)|^2r^{d-1}\,\mathrm{d}r-1\right). \tag{10}$$

Considering the perturbation $\phi \to \phi + \varepsilon\varphi$ (ε be a small real parameter and φ be an arbitrary differentiable test function), we then compute the corresponding variations with respect to the kinetic, potential, nonlinear, and normalization terms:

$$\begin{aligned}
&\delta\left(\frac{1}{2}\int_0^\infty \left|\frac{\mathrm{d}\phi}{\mathrm{d}r}\right|^2 r^{d-1}\mathrm{d}r\right)\\
&= -\mathrm{Re}\left(\int_0^\infty \overline{\varphi}\frac{\mathrm{d}}{\mathrm{d}r}\left(r^{d-1}\frac{\mathrm{d}\phi}{\mathrm{d}r}\right)\mathrm{d}r\right),\\
&\delta\left(\frac{1}{2}\int_0^\infty V(r)|\phi|^2 r^{d-1}\mathrm{d}r\right)\\
&= \mathrm{Re}\left(\int_0^\infty \overline{\varphi}V(r)\phi r^{d-1}\mathrm{d}r\right),\\
&\delta\left(\frac{\beta}{2}\int_0^\infty |\phi|^4 r^{d-1}\mathrm{d}r\right)\\
&= 2\beta\mathrm{Re}\left(\int_0^\infty \overline{\varphi}|\phi|^2\phi r^{d-1}\mathrm{d}r\right),\\
&\delta\left(\frac{\mu}{2}\int_0^\infty |\phi|^2 r^{d-1}\mathrm{d}r\right)\\
&= \mu\mathrm{Re}\left(\int_0^\infty \overline{\varphi}\phi r^{d-1}\mathrm{d}r\right),
\end{aligned} \tag{11}$$

where $\overline{\varphi}$ denotes the complex conjugate of ϕ.

By combining the variations of all terms, we obtain

$$\begin{aligned}
\delta\mathcal{L} = \mathrm{Re}\int_0^\infty \overline{\varphi}\Big[&-\frac{\mathrm{d}}{\mathrm{d}r}\left(r^{d-1}\frac{\mathrm{d}\phi}{\mathrm{d}r}\right)+V(r)\phi r^{d-1}\\
&+2\beta|\phi|^2\phi r^{d-1}-\mu\phi r^{d-1}\Big]\mathrm{d}r = 0.
\end{aligned} \tag{12}$$

The first variation condition $\delta L = 0$ leads to the time-independent (stationary) GPE (5). Therefore, the minimizer of the energy functional $E(\phi)$ under the normalization constraint must satisfy the stationary Gross–Pitaevskii equation and corresponds to the ground state of the system. The same variational approach can be extended to systems with cylindrical symmetry.

2.2. The cylindrical symmetric ground state

We also solve the GPE under cylindrical symmetry in this paper. Due to the symmetry, the 3D GPE is reduced to a two-dimensional problem

$$\begin{aligned}
\mathrm{i}\frac{\partial\psi(r,z,t)}{\partial t} = &-\frac{1}{2}\left[\frac{1}{r}\frac{\partial}{\partial r}\left(r\frac{\partial\psi}{\partial r}\right)+\frac{\partial^2\psi}{\partial z^2}\right]\\
&+V(r,z)\psi+\beta|\psi|^2\psi,
\end{aligned} \tag{13}$$

where $r=\sqrt{x^2+y^2}$ and $V(r,z)=\frac{1}{2}\left(r^2+\gamma_z^2 z^2\right)$ (i.e., $\gamma_z^2=1$). The energy functional $E(\phi)$ with cylindrical symmetry is defined as follows:

$$\begin{aligned}
E(\phi) = 4\pi\int_0^\infty\int_0^\infty r\Big[&\frac{1}{2}\left(\phi_r^2(r,z)+\phi_z^2(r,z)\right)\\
&+\left(r^2+\gamma_z^2 z^2\right)\phi^2(r,z)+\beta\phi^4(r,z)\Big]\mathrm{d}r\mathrm{d}z.
\end{aligned} \tag{14}$$

The boundary conditions are set as

$$\begin{aligned}
&\frac{\partial\phi(0,z)}{\partial r}=0, \quad 0\le z<\infty,\\
&\frac{\partial\phi(r,0)}{\partial z}=0, \quad 0\le r<\infty,\\
&\phi(r,z)\to 0, \ \text{ when } \ r+|z|\to\infty.
\end{aligned}$$

The ground state of the GPE (9) can be obtained by solving the minimization problem

$$E_\beta(\phi_g) = \min_{\phi\in V} E_\beta(\phi). \tag{15}$$

Under the normalization conditions

$$4\pi\int_0^\infty\int_0^\infty |\phi(r,z)|^2 r\mathrm{d}r\mathrm{d}z = 1, \tag{16}$$

the energy functional $E(\phi)$ is inherently dimension-independent: its mathematical form (Eq. (7)) holds for any spatial dimension d, with adjustments only to coordinate systems (e.g., radial weights r^{d-1}) and symmetry constraints. While the variational principle is universal, practical applications require validation across dimensions to address real-world quantum systems (e.g., 3D BECs[4]) and numerical challenges in high-dimensional spaces.

3. Residual neural network for ground state

3.1. Network architectures

Residual neural network is used primarily due to its ability to efficiently handle vanishing or exploding gradients in deep networks.[22] In this paper, the ResNet combined with physical laws is applied to solve the ground state problem of BEC.

We first briefly introduce the ResNet architecture

$$\begin{aligned}
f_\theta(x) = &F_{L+1}\circ(F_L+I)\circ(F_{L-1}+I)\circ\cdots\circ\\
&(F_2+I)\circ(F_1+I)(x),
\end{aligned} \tag{17}$$

where $(F_l+I)(x)=F_l(x)+x$ and

$$F_l(x) = W_{l,2}\cdot\sigma\left(W_{l,1}\cdot x+b_{l,1}\right)+b_{l,2}.$$

The network $f_\theta(x)$ consists of L residual blocks and a final output layer. Each residual block (F_l+I) combines a nonlinear transformation F_l with an identity mapping I, connected through the function composition operator $\circ$. Here $F_l(x) = W_{l,2}\sigma\left(W_{l,1}x+b_{l,1}\right)+b_{l,2}$ with weight matrices $W_{l,i}\in R^{n_l\times n_{l-1}}$, bias vectors, $b_{l,i}\in R^{n_l}$, and activation function σ (e.g., tanh). Batch normalization is applied in each block to stabilize training. The input x (spatial coordinates) passes through the blocks to produce the output. The structure is shown in Fig. 1.

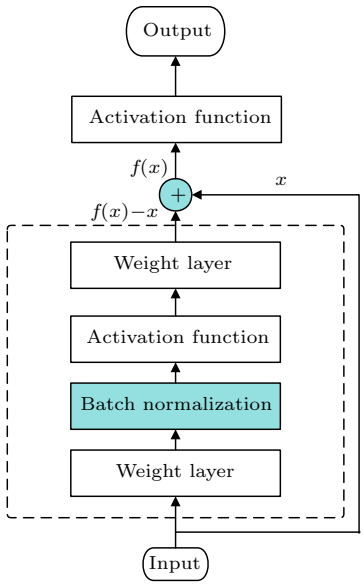


Fig. 1. The residual block comprises two fully connected layers with batch normalization and tanh activation.

The full network architecture, based on residual blocks, is shown in Fig. 2. We use Xavier normal initialization[23] for weights and set all biases to zero. Three activation functions are used: cosine in the first layer to capture symmetry, tanh in the residual blocks for stable gradients, and Softplus in the output layer to ensure non-negative density. These choices of activation functions are tailored to the specific requirements of the problem, ensuring that the network respects symmetry, trains efficiently, and produces physically meaningful outputs. A final normalization layer N is added to enforce the quantum constraint. The definition of N is as follows:

$$N(y) = y/\|y\|_2,$$

where y is output from the Softplus layer, and $\|y\|_2 = \sqrt{C_d \int_\Omega |y|^2 x^{d-1}\,\mathrm{d}x}$.

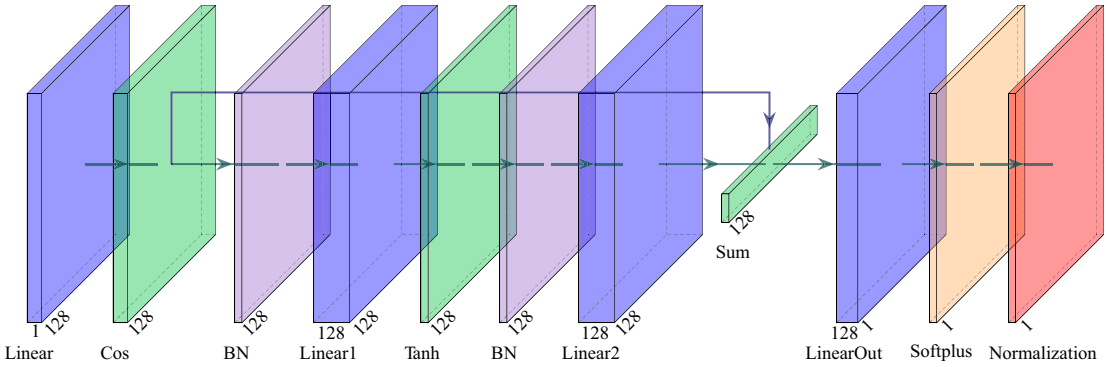


Fig. 2. Energy-minimizing normalized residual network.

3.2. Loss function

The loss function combines two physics-driven components: an energy loss minimizing the GPE energy functional, and a boundary loss enforcing Neumann/Dirichlet conditions. This design ensures solutions simultaneously satisfy energy minimization and wavefunction confinement.

$$L_{\text{energy}} = \int \left(\frac{1}{2} |\nabla \psi|^2 + V(x) |\psi|^2 + \frac{\beta}{2} |\psi|^4 \right) \mathrm{d}x. \quad (18)$$

The radially symmetric boundary conditions are crucial for physical consistency: the Neumann condition $\partial\psi/\partial r|_{r=0} = 0$ ensures smoothness at the origin, while the Dirichlet condition $\psi(R) = 0$ enforces confinement at the boundary. These physical constraints are implemented via a boundary loss term, which is defined as

$$L_{\text{boundary}} = (\partial\psi/\partial r|_{r=0})^2 + (\psi(R))^2. \quad (19)$$

The total loss L_{total} is the weighted sum of the energy and boundary losses

$$L_{\text{total}} = \alpha_1 L_{\text{energy}} + \alpha_2 L_{\text{boundary}}, \quad (20)$$

where α_i are weights balancing the importance of each term. This formulation ensures that the network learns solutions consistent with the physics of the GPE while satisfying the necessary boundary conditions.

3.3. Optimizer and gradient clipping

Choosing an optimizer for ResNet depends on task complexity, data size, and network structure. Common choices include Adam, SGD, and RMSProp.[24,26] In this paper, we use Adam for its adaptive learning rate and strong performance on non-convex problems. The initial learning rate is 10^{-3}, with L_2 regularization (weight decay 10^{-5}) to reduce overfitting. An exponential decay lowers the learning rate by 0.99 every 200 steps, ensuring stable and gradual convergence.

To ensure training stability, we also employ a gradient clipping strategy to prevent gradient explosion. This approach rescales gradients when their norm exceeds a threshold C. The formula for gradient clipping is as follows:

$$g_{\text{clipped}} = \frac{C}{||g||} \cdot g \quad \text{if} \quad ||g|| > C,$$
$$g_{\text{clipped}} = g \quad \text{if} \quad ||g|| \le C.$$

where g is the gradient of the parameters. C is the gradient threshold (a hyperparameter). g_{clipped} is the clipped gradient.

3.4. The training strategy

To solve the ground state solution of GPE, a two-stage training strategy is proposed. The strategy approximates the wave function by embedding physical constraints and dynamic optimization mechanism. The specific process is shown in Fig. 3.

The steps involved in obtaining the ground solution using the EM-NormResNet algorithm are as follows.

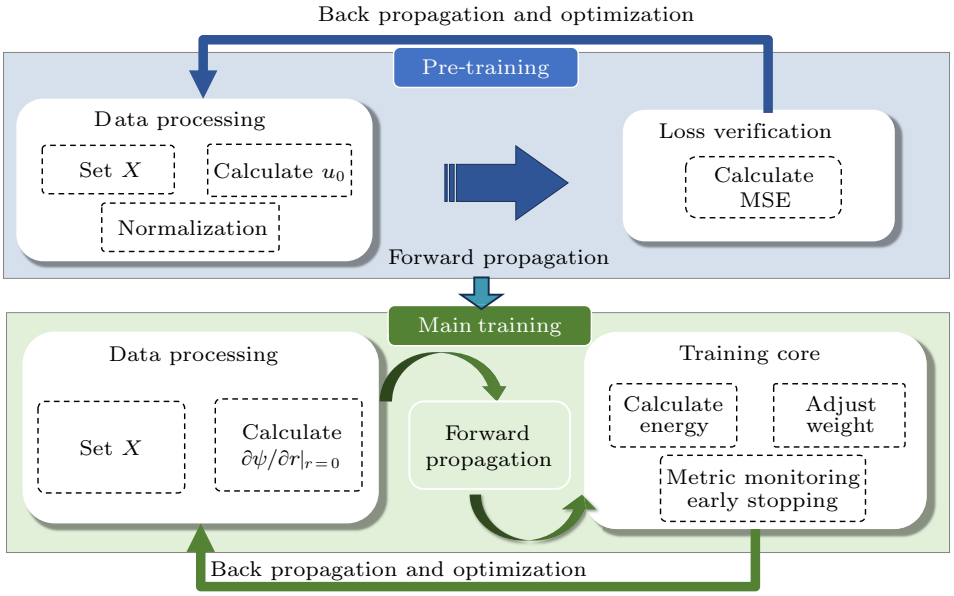


Fig. 3. Training strategy flowchart.

3.4.1. Pre-training

Generate a uniformly distributed set of points $X = r_i$ in the interval.

Calculate the initial wave function $u_0 = \phi_d^s(r)$ in Eq. (21). Design the loss function by the mean square error loss $= \sum (U_{\text{pred}} - U_0)^2$.

Select the neural network parameters: number of hidden layers and number of neurons per layer, activation function, optimizer type and the number of iterations for the minimization.

3.4.2. Main-training

Generate a uniformly distributed set of points $X = r_i$ in the interval and boundary integration points.

Design the loss function for the interior points and the boundary as stated in Eq. (20).

Select the neural network parameters for the minimization.

Track energy $E(\phi)$ and normalization error δ_{norm} in real time. If average energy $\Delta E < (\xi = 10^{-6})$ and $\delta_{\text{norm}} < 10^{-4}$ for 100 consecutive steps, convergence is determined and training is terminated.

4. Numerical results

This section reports that EM-NormResNet can accurately compute GPE ground states in 1D, 2D (radial) and 3D (cylindrical) systems. By varying network depth, grid size, and normalization techniques, we show that the method effectively preserves energy and accuracy, overcomes numerical challenges arising from symmetry, and enforces the required physical constraints.

4.1. Ground-state solution of radially symmetric case 1D

The potential $V(\boldsymbol{x})$ in Eq. (1) is set as $V(x) = \frac{1}{2}x^2$, and the hyper-parameters are set as follows: spatial interval [0,16], interaction strength $\beta = 627.42$, tolerance $\xi = 10^{-6}$, with pre-training steps of 2000 and main training steps of 2000.

To enhance training efficiency and accuracy, we designed a pretraining process for the ResNet method. The target values $\phi_d^s(r)$ are chosen as[15]

$$\phi_d^s(r) = \begin{cases} \sqrt{\left(\mu_g^s - \frac{r^2}{2}\right)/\beta}, & r^2 < 2\mu_d^s, \quad d = 1,2,3, \\ 0, & \text{otherwise}, \end{cases} \tag{21}$$

where

$$\mu_d^s = \frac{1}{2}\left[\frac{\left((d+1)^2 - 1\right)\beta}{C_d}\right]^{2/(d+2)}, \quad d = 1,2,3. \tag{22}$$

4.1.1. Influence of network architecture

Here we test $L \in \{1,2,3,4\}$, $W \in \{10,70,128\}$. Figure 4(a) shows $\phi(x)$ for different network architectures; figure 4(b) displays energy E_β over epochs; figure 4(c) shows the

absolute error. Table 1 reports the maximum pointwise error and energy error for each depth and width.

Figure 4 and Table 1 show that deeper and wider networks cut the max error from 5.78×10^{-2} to 9.08×10^{-3} and the energy error from 4.23×10^{-1} to 2.96×10^{-3}. As β grows, the wave's peak drops and its profile widens, balancing interaction and kinetic energy. When interactions are strong, $|\phi|^2$ becomes almost flat, following $|\phi|^2 \approx (\mu - V)/\beta$.[15] The network minimizes $E(\phi)$ (Eq. (8)), by trading off $(|\phi|^4)$ and $(|\nabla\phi|^2)$.

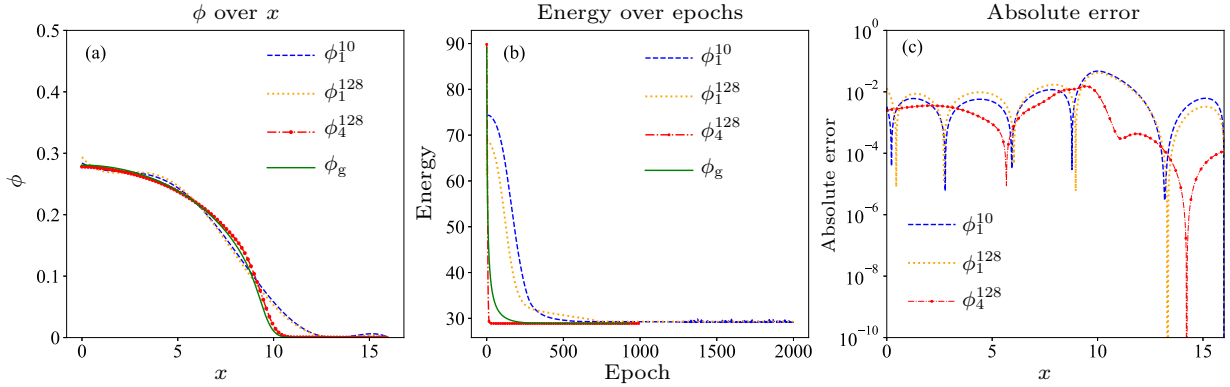


Fig. 4. EM-NormResNet with different network architectures: (a) exact solution and numerical solution; (b) exact energy and numerical energy; (c) absolute errors of different architectures.

Table 1. Maximum pointwise error and energy error for EM-NormResNet with varying architectures (layer depth L and width W).

	L \ W	10	70	128
$\max\left\|\phi(x)-\phi_g(x)\right\|$	1	5.78×10^{-2}	5.01×10^{-2}	5.19×10^{-2}
	2	2.73×10^{-2}	2.02×10^{-2}	2.06×10^{-2}
	3	1.88×10^{-2}	1.20×10^{-2}	1.09×10^{-2}
	4	1.52×10^{-2}	1.02×10^{-2}	9.08×10^{-3}
$\left\|E_\beta(\phi)-E_\beta(\phi_g)\right\|$	1	4.23×10^{-1}	4.41×10^{-1}	4.36×10^{-1}
	2	1.97×10^{-1}	1.40×10^{-1}	1.39×10^{-1}
	3	1.83×10^{-1}	1.37×10^{-1}	1.34×10^{-1}
	4	1.42×10^{-1}	1.32×10^{-1}	2.96×10^{-2}

4.1.2. Influence of grid size

Then we examine the effect of the grid ($N_x \in 10, 100, 1000$). Figure 5(a) shows the wave function $\phi(x)$, figure 5(b) displays the energy E_β versus epochs, and figure 5(c) presents the absolute error. Table 2 lists the maximum pointwise and energy errors for each grid, isolating the effect of resolution on accuracy.

Figure 5 and Table 2 show that increasing the grid from $Nx = 10 \to 1000$ cuts the maximum error from 1.03×10^{-1} to 9.08×10^{-3} and the energy error from 1.96×10^{1} to 2.96×10^{-2}. Finer meshes resolve the sharp edge gradients, while coarse ones break the kinetic–interaction energy balance. High resolution is therefore vital for accurate results, especially under strong interactions.

Table 2. Maximum pointwise error and energy error for EM-NormResNet with varying grid.

Grid size (N_x)	10	100	1000
$\max\left\|\phi(x)-\phi_g(x)\right\|$	1.03×10^{-1}	9.51×10^{-2}	9.08×10^{-3}
$\left\|E_\beta(\phi)-E_\beta(\phi_g)\right\|$	1.96×10^{1}	4.71×10^{-2}	2.96×10^{-2}

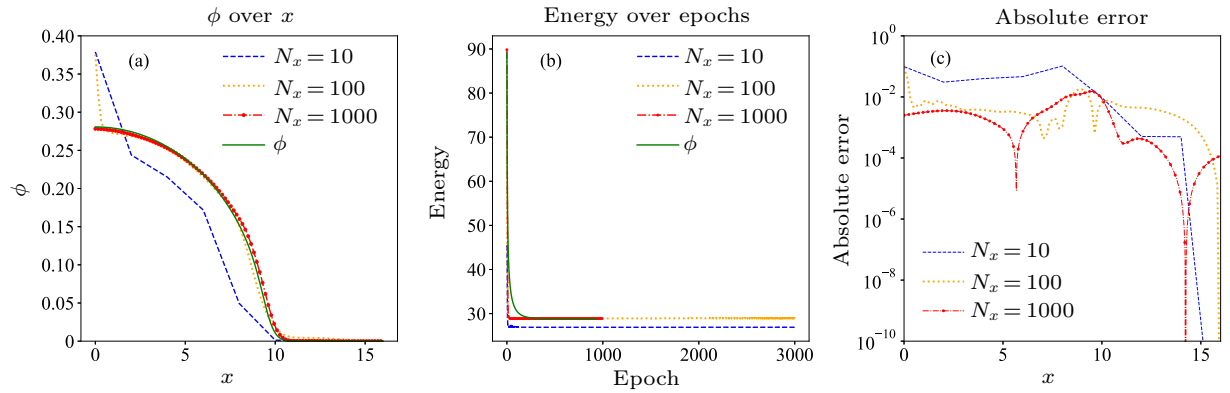


Fig. 5. EM-NormResNet with different grid resolutions. (a) is the comparison between the exact solution and numerical solutions; (b) is the energy values over training epochs; (c) is the absolute error of ϕ for different grid resolutions.

4.1.3. Influence of normalization layer

We next present numerical experiments to compare the impact of the normalization loss function on the numerical results. Figure 6 shows the ground state, the energy and the absolute error with and without normalization.

Table 3 presents the numerical energy $E(\phi)$ for different network depths and widths with and without a normalization layer.

By incorporating the normalization loss term, we observe a significant improvement in both energy conservation and accuracy. The normalization ensures that the computed wave function adheres to the physical constraint of normalization, which leads to more stable and reliable results. For example, when $L=4$ and $W=128$, the normalized model gives $E=28.883$, close to the exact $E(\phi_{\mathrm{g}})=28.849$, while the unnormalized model yields 27.132. These improvements highlight the importance of including the normalization term in the loss function for better precision and physical consistency in solving the Gross–Pitaevskii equation.

Table 3. Numerical energy $E(\phi)$ for 1D problem with or without normalization layer, exact $E(\phi_{\mathrm{g}})=28.849$.

$E(\phi)$	L \ W	10	70	128
With normalization	1	29.212	29.200	29.290
	2	29.914	28.993	28.983
	3	29.722	28.228	28.985
	4	28.983	28.891	28.883
Without normalization	1	15.756	17.531	17.449
	2	24.245	26.680	26.843
	3	23.183	27.123	26.962
	4	27.005	26.977	27.132

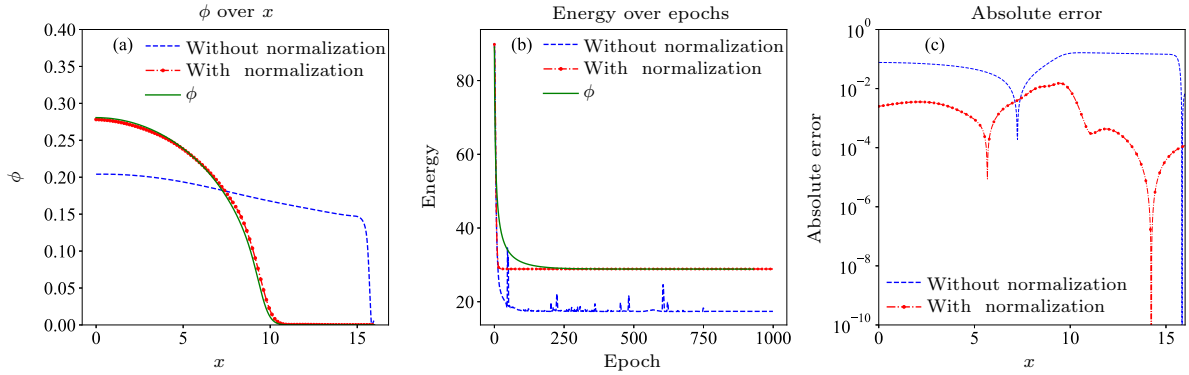


Fig. 6. EM-NormResNet with or without normalization: (a) is the comparison between the exact solution and numerical solutions; (b) is the energy values over training epochs; (c) is the absolute error of ϕ for different grid resolutions.

4.2. Ground-state solution of 2D radially symmetric case

We calculate the maximum values, L_2 norm, and energy errors for different values of β in the two-dimensional radially symmetric case. The results are listed in Table 4. The ground-state numerical solutions and error curves are shown in Fig. 7. When $\beta=50$, the exact and numerical solutions, along with the corresponding energy evolution, are depicted in Fig. 8.

From these tables and figures, we observe that the peak of the ground-state solution decreases as the interaction coefficient β increases. This behavior is expected, as a larger value of β corresponds to a stronger inter-particle interaction in the

Table 4. Numerical error analysis of different β for 2D.

	$\beta=50$	$\beta=100$	$\beta=313.71$	$\beta=627.42$	$\beta=1254.8$
$\max\lvert\phi(x)-\phi_{\mathrm{g}}(x)\rvert$	6.73×10^{-3}	4.71×10^{-3}	1.01×10^{-2}	1.12×10^{-3}	3.76×10^{-3}
$\lVert\phi-\phi_{\mathrm{g}}\rVert_{L^2(\Omega)}$	6.05×10^{-2}	4.64×10^{-2}	1.00×10^{-1}	2.89×10^{-2}	4.68×10^{-2}
$\lvert E_\beta(\phi)-E_\beta(\phi_{\mathrm{g}})\rvert$	3.40×10^{-3}	3.05×10^{-2}	2.15×10^{-2}	4.42×10^{-2}	4.10×10^{-3}

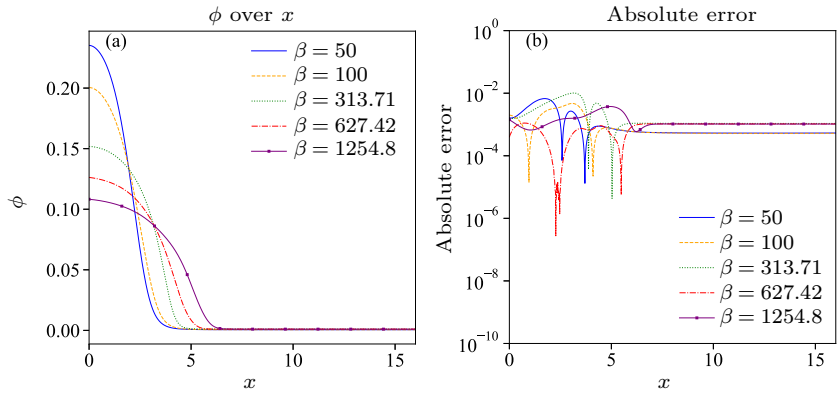


Fig. 7. Ground-state wave function (a) and absolute error (b) in 2D with radial symmetry for varying interaction strengths β.

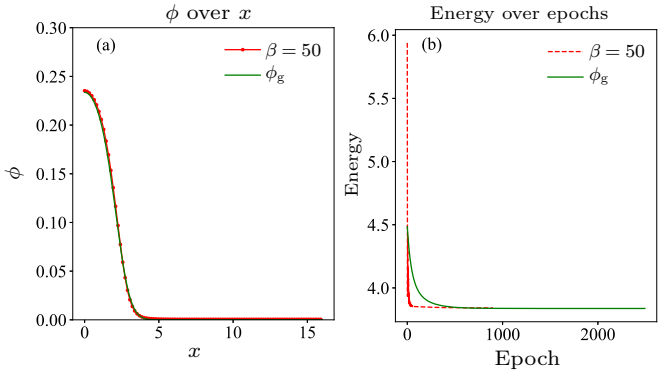


Fig. 8. EM-NormResNet for 2D with radial symmetry: exact solution and numerical solution; exact energy and numerical energy. (a) is the ϕ over x, (b) is the energy over epochs.

system, which tends to compress the wave function, thus reducing its peak. This trend reflects the physical influence of the nonlinearity introduced by β, which governs the strength of the attractive or repulsive interactions between particles in the Bose–Einstein condensate.

4.3. Ground-state solution of 3D spherical symmetric case

Similarly, we perform calculations for the three-dimensional axially symmetric case, extending the analysis to higher dimensions. In this setup, we investigate the effects of varying parameters on the ground-state solution, including the interaction coefficient β, and analyze the resulting numerical solutions and associated errors. See Figs. 9, 10, and Table 5. This allows us to further validate the robustness of the model and explore the behavior of the system in three-dimensional space.

Table 5. Numerical error analysis of different β for 3D.

	$\beta = 50$	$\beta = 100$	$\beta = 313.71$	$\beta = 627.42$	$\beta = 1254.8$
$\max\left\|\phi(x) - \phi_g(x)\right\|$	1.27×10^{-2}	1.46×10^{-2}	1.02×10^{-2}	6.48×10^{-3}	4.15×10^{-3}
$\left\|\phi - \phi_g\right\|_{L^2(\Omega)}$	1.17×10^{-1}	1.20×10^{-2}	8.14×10^{-2}	5.13×10^{-2}	3.74×10^{-2}
$\left\|E_\beta(\phi) - E_\beta(\phi_g)\right\|$	3.40×10^{-3}	2.62×10^{-2}	2.84×10^{-2}	2.75×10^{-2}	2.78×10^{-3}

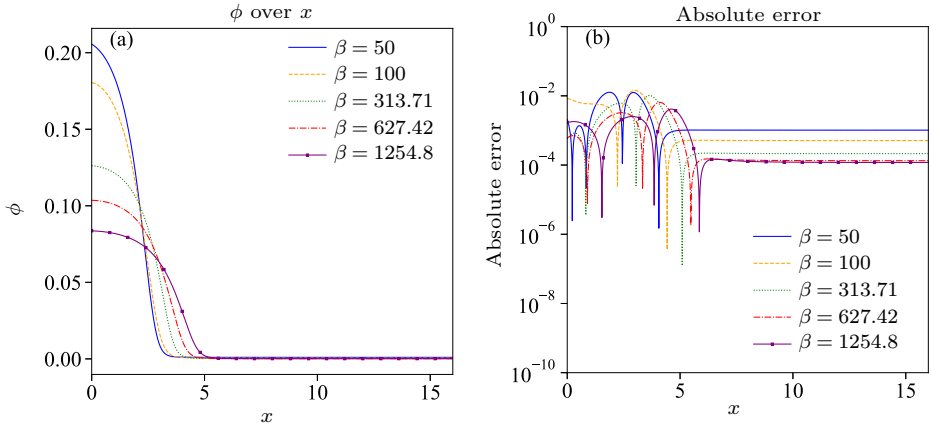


Fig. 9. Ground-state wave function (a) and absolute error (b) in 3D with spherical symmetry for varying interaction strengths β.

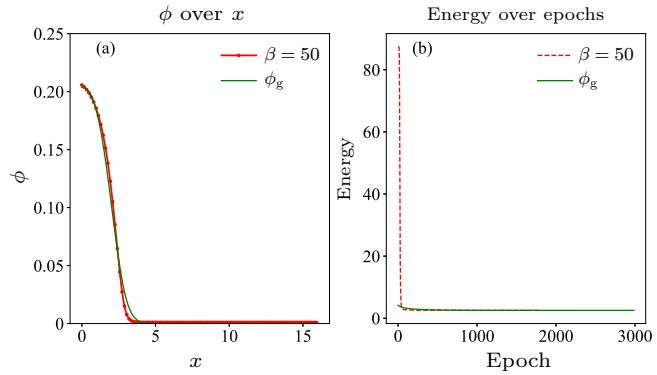


Fig. 10. EM-NormResNet for 3D with spherical symmetry: exact solution and numerical solution; exact energy and numerical energy. (a) is the ϕ over x, (b) is the energy over epochs.

4.4. Ground-state solution of 3D cylindrical symmetry case

In this section, we present the neural network approximation for the ground-state solution of GPE in 3D with cylindrical symmetry. The initialization settings for strong repulsive interactions are[15]

$$\mu_1^s = \frac{1}{2}\left(\frac{15\beta\gamma_z}{4\pi}\right)^{2/5}, \tag{23}$$

$$\phi_1^s(r,z)\begin{cases}\sqrt{\left(\mu_1^s - \frac{r^2+\gamma_z^2 z^2}{2}\right)/\beta}, & r^2+\gamma_z^2 z^2 < 2\mu_1^s,\\ 0, & \text{otherwise.}\end{cases} \tag{24}$$

Next, we consider the three-dimensional cylindrically symmetric case, where the GPE can be effectively approximated using the two-dimensional equation. We compute the curves along the r-axis and z-axis for different values of β, as shown in Fig. 11. Figure 12 presents the ground-state numerical surface plot for $\beta = 31.371$, along with the corresponding energy evolution over time.

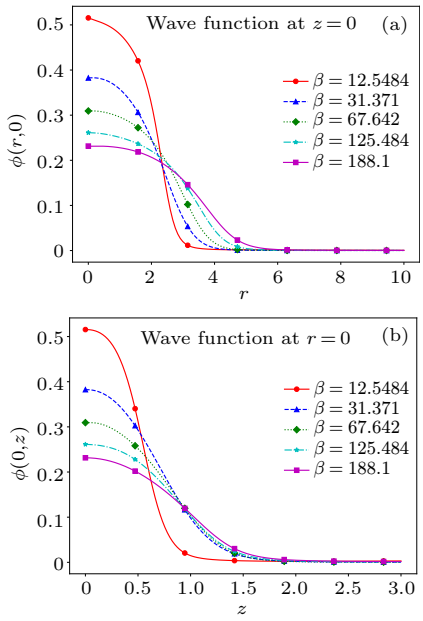


Fig. 11. Ground-state solution in 3D with cylindrical symmetry: (a) is the wave function at $z = 0$, (b) is the wave function at $r = 0$.

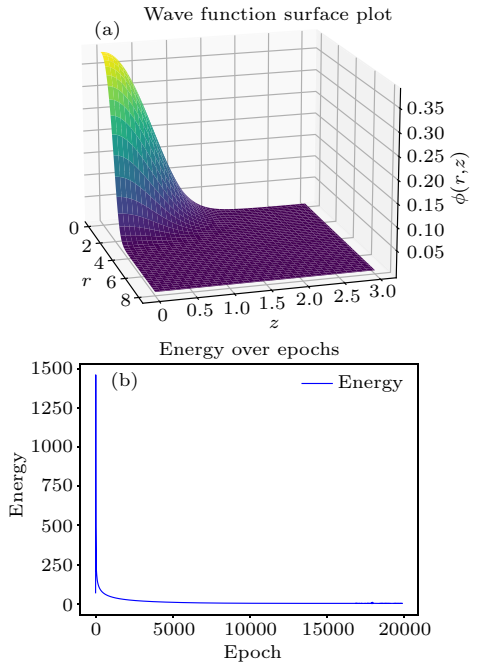


Fig. 12. (a) Surface plots of the condensate wave function $\beta = 31.371$ and (b) the energy evolution during training.

From these figures, we observe that as the interaction strength β increases, the spatial distribution of the wave function becomes more compressed, especially in the radial direction. This suggests that stronger interactions lead to a tighter confinement of the condensate. Additionally, the energy curve indicates a stabilization of the system over time, with the energy approaching a steady state, which confirms the convergence of the numerical solution to the ground state. The evolution of the energy reflects the system's relaxation process towards equilibrium, which is influenced by the magnitude of β.

5. Conclusion

In this paper, we develop an energy-minimizing normalized residual network approach to solve the ground-state solutions of the GPE in one, two dimensions (with radial symmetry), and three dimensions (with cylindrical symmetry). Our approach employs neural networks and incorporates physical constraints through the energy functional and boundary conditions. The symmetry reduces the computational complexity while preserving the essential physics via proper volume elements and normalization factors. The results demonstrate accurate predictions of ground-state wave functions across different interaction strengths. Future work could extend this framework to excited states and time-dependent dynamics of the system.

Acknowledgement

Project supported by the National Natural Science Foundation of China (Grant No. 11971411).

References

[1] Luo X Y, Zou Y Q, Wu L N, Liu Q, Han M F, Meng K T and You L 2017 *Science* **355** 620
[2] Anderson M H, Ensher J R, Matthews M R, Wieman C E and Cornell E A 1995 *Science* **269** 198
[3] Erdos L, Schlein B and Yau H 2007 *Phys. Rev. Lett.* **98** 040404
[4] Bao W Z and Du Q 2004 *SIAM J. Sci. Comput.* **25** 1674
[5] Gauthier G, Reeves M T, Yu X Q, Bradley A S, Baker M A, Bell T A, Rubinsztein-Dunlop H, Davis M J and Neely T W 2019 *Science* **364** 1264
[6] Shukla P K and Eliasson B 2007 *Phys. Rev. Lett.* **99** 096401
[7] Hasegawa A and Tappert F 1973 *Appl. Phys. Lett.* **23** 171
[8] Chiofalo M L, Succi S and Tosi M P 2000 *Phys. Rev. E.* **62** 7438
[9] Danaila I and Kazemi P 2010 *SIAM J. Sci. Comput.* **32** 2447
[10] Danaila I and Protas B 2017 *SIAM J. Sci. Comput.* **39** B1102
[11] Bao W Z, Chang Z P and Zhao X F 2025 *J. Comput. Phys.* **520** 113486
[12] Ruprecht P A, Holland M J, Burnett K and Edwards M 1995 *Phys. Rev. A.* **51** 4704
[13] Muruganandam P and Adhikari S K 2002 *J. Phys. B* **35** 2831
[14] Caliari M, Ostermann A, Rainer S and Thalhammer M 2009 *J. Comput. Phys.* **228** 349
[15] Bao W and Tang W 2003 *J. Comput. Phys.* **187** 230
[16] Evrard B, Qu A, Dalibard J and Gerbier F 2021 *Science* **373** 1340
[17] Raissi M, Perdikaris P and Karniadakis G E 2018 *J. Comput. Phys.* **378** 686
[18] Jagtap A D, Kawaguchi K and Karniadakis G E 2020 *J. Comput. Phys.* **404** 109136
[19] Zhang Z, Li J and Liu B 2025 *J. Comput. Phys.* **521** 113561
[20] Tian S, Cao C and Li B 2023 *Results Phys.* **52** 106842
[21] E W and Yu B 2018 *Commun. Math. Stat.* **6** 1
[22] He K, Zhang X, Ren S Q and Sun J 2016 Deep Residual Learning for Image Recognition[C] 2016 *IEEE Conference on Computer Vision and Pattern Recognition (CVPR)*, June 27–30, 2016 Las Vegas, NV, USA, p. 770
[23] Glorot X and Bengio Y 2010 *J. Mach. Learn. Res.* **9** 249
[24] Kingma D P and Ba J L 2014 arXiv:1412.6980v1 [cs.LG]
[25] Tian Y, Zhang Y and Zhang H 2023 *Mathematics* **11** 682
[26] Mukkamala M C and Hein M 2017 arXiv:1706.05507 [cs.LG]